Effective LAI and CHP of a single tree from small-footprint full-waveform LiDAR

Article

Published Version

Effective LAI and CHP of a Single Tree From Small-Footprint Full-Waveform LiDAR

Karolina D. Fieber, Ian J. Davenport, Mihai A. Tanase, James M. Ferryman, Robert J. Gurney, Jeffrey P. Walker, and Jorg M. Hacker

***Abstract*—This letter has tested the canopy height profile (CHP) methodology as a way of effective leaf area index (LAI_e) and vertical vegetation profile retrieval at a single-tree level. Waveform and discrete airborne LiDAR data from six swaths, as well as from the combined data of six swaths, were used to extract the LAI_e of a single live *Callitris glaucophylla* tree. LAI_e was extracted from raw waveform as an intermediate step in the CHP methodology, with two different vegetation-ground reflectance ratios. Discrete point LAI_e estimates were derived from the gap probability using the following: 1) single ground returns and 2) all ground returns. LiDAR LAI_e retrievals were subsequently compared to hemispherical photography estimates, yielding mean values within $\pm 7\%$ of the latter, depending on the method used. The CHP of a single dead *Callitris glaucophylla* tree, representing the distribution of vegetation material, was verified with a field profile manually reconstructed from convergent photographs taken with a fixed-focal-length camera. A binwise comparison of the two profiles showed very high correlation between the data reaching R^2 of 0.86 for the CHP from combined swaths. Using a study-area-adjusted reflectance ratio improved the correlation between the profiles, but only marginally in comparison to using an arbitrary ratio of 0.5 for the laser wavelength of 1550 nm.**

***Index Terms*—Canopy height profile (CHP), effective leaf area index (LAI_e), full-waveform airborne LiDAR, single tree, Soil Moisture Active Passive Experiment (SMAPEx), vegetation profile.**

I. Introduction

KNOWLEDGE of canopy structure is important in the understanding of forest ecosystems functioning [1]. How the foliage is arranged in 3-D space determines the interaction between vegetation and atmosphere and drives the exchange of energy between them [2], [3]. Canopy structure is often parameterized by vegetation indices such as the leaf area index (LAI). LAI, defined as half the total leaf area per unit ground area [4], changes with height within the canopy, and this variation is often characterized as vertical foliage profiles [5], [6]. Due to its 3-D character, LiDAR data have been found particularly suited for the description of vegetation architecture by many scientists [7]–[9]. Data from a range of platforms have been tested for LAI retrieval. Recently, some attention has been given to full-waveform laser scanners, which, in contrast to discrete systems, provide the entire recording of the reflected energy from the targets in the laser path. They therefore facilitate the retrieval of vertical vegetation distribution directly from the returned light curve.

Indirect methods of LAI estimation, such as LiDAR or hemispherical photography, rely on the gap fraction approach, which assumes the random distribution of canopy elements. In reality, this assumption is often violated, particularly for coniferous trees for which clumping appears at several levels. Furthermore, indirect methods do not differentiate between woody and foliar elements of vegetation. To emphasize the difference between true LAI value and indirect estimates, several terms have been used in the literature. These include plant area index, vegetation area index, and effective LAI (LAI_e). The latter term, proposed in [10] and following suggestions in [2], is the most suitable for this particular study since the LAI techniques here have not been corrected for clumping or contribution of woody elements.

Most studies focus on plot- and site-level LAI and foliage profile retrievals. With the availability of small-footprint full-waveform laser data, it is now possible to retrieve them at a much smaller scale, such as a single tree. In this letter, the previously developed methodology of the Scanning Lidar Imager of Canopies by Echo Recovery (SLICER) canopy height profile (CHP) [7] adapted to small-footprint LiDAR data by Fieber *et al.* [11] is tested for the extraction of LAI_e and CHP of two single trees. To compensate for the small number of trees tested (due to ground-truth data limitations), six independent swaths of LiDAR data are used for the analysis. The raw-waveform method based on CHP processing, as well as two discrete point methods, is contrasted and compared to hemispherical photography LAI_e estimates of a live *Callitris glaucophylla* tree. A CHP of a dead *Callitris glaucophylla* tree is validated against a "field" tree profile, reconstructed based on convergent photographs taken in the field with a fixed-focal-length camera. This letter aims to assess the suitability of the CHP approach for LAI_e and vegetation profile retrieval from small-footprint LiDAR data at a single-tree level.

Manuscript received September 4, 2013; revised October 4, 2013 and January 22, 2014; accepted January 24, 2014. This work was supported in part by the Engineering and Physical Sciences Research Council under Grant EP/P505682/1 and in part by the School of Mathematical and Physical Sciences and School of Systems Engineering of the University of Reading, U.K. The data used in the study were acquired as part of the Third Soil Moisture Active Passive experiment (SMAPEx-3) and funded by Australian Research Council Projects LE0560930, DP09845861, and FS100100040. The waveform processing was funded by the National Centre for Earth Observation, U.K. The 2012 data set was funded by Airborne Research Australia.

K. D. Fieber and J. M. Ferryman are with the School of Systems Engineering, University of Reading, Reading RG6 6AY, U.K. (e-mail: k.fieber@pgr.reading.ac.uk).

I. J. Davenport and R. J. Gurney are with the School of Mathematical and Physical Sciences, University of Reading, Reading RG6 6AL, U.K.

M. A. Tanase is with the University of Melbourne, Melbourne, Vic. 3010, Australia.

J. P. Walker is with the Faculty of Engineering, Monash University, Melbourne, Vic. 3800, Australia.

J. M. Hacker is with the Airborne Research Australia, School of Environment, Flinders University, Adelaide, S.A. 5001, Australia.

Color versions of one or more of the figures in this paper are available online at http://ieeexplore.ieee.org.

Digital Object Identifier 10.1109/LGRS.2014.2303500

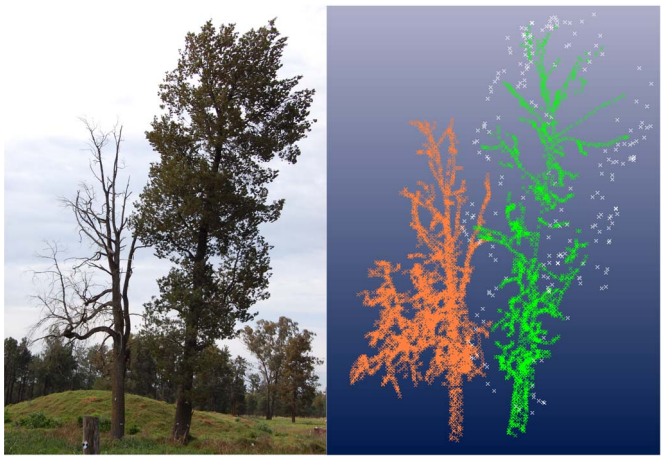

Fig. 1. Left: Terrestrial photography of the two *Callitris glaucophylla* trees. Right: Reconstruction of the tree structure in PhotoModeler (orange = dead tree, green = live tree structure, white = leaves).

II. Study Area and Data

The study area is located in the Gillenbah forest, close to the town of Narrandera, in New South Wales, Australia. It is a relatively sparse white cypress pine (*Callitris glaucophylla*) forest with a small proportion (less than 10%) of Grey Box (*Eucalyptus microcarpa*). Two single *Callitris glaucophylla* trees, one live and one dead, were chosen for this study (see Fig. 1). The trees are growing next to each other and are located at 55454654E, 6147221S, in the center of the forest. Field measurements and five swaths of LiDAR data over the study area were acquired during the Soil Moisture Active Passive Experiment 3 (SMAPEx-3) in September 2011 [12]. The last swath of LiDAR data, courtesy of Airborne Research Australia (ARA), was acquired in December 2012.

A. Field Data

During the site visit on September 16, 2011, the height of both trees was measured using a clinometer. Convergent photographs were taken around the trees with a fixed-focal-length Nikon D40 camera to enable manual tree structure reconstruction by photogrammetric means. Additionally, hemispherical upward-pointing photographs of the live *Callitris glaucophylla* were taken in four cardinal directions in order to facilitate the estimation of the LAI_e.

B. LiDAR Data

All LiDAR data over the study area were acquired with a RIEGL LMS-Q560 full-waveform scanner by ARA. Both transmitted and received waveforms were recorded with a frequency of 1 GHz (1-ns spacing). The area of the two trees was covered by six LiDAR swaths, each with an average shot density of 9 points/m^2. Three of the swaths were acquired on September 6, 2011, two on September 22, 2011, and the last swath on December 19, 2012. In SMAPEx-3 acquisition, the laser instrument was mounted on a light aircraft and flown at 350 m above ground level (AGL), resulting in a 0.175-m footprint diameter. The 2012 LiDAR was flown at 300 m AGL,

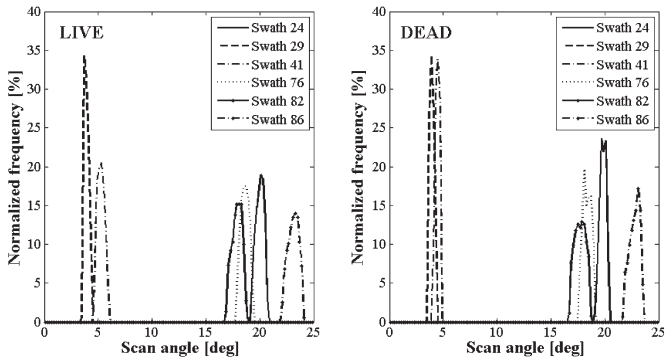

Fig. 2. Histograms of scan angle distributions for six swaths for (left) live and (right) dead *Callitris glaucophylla*.

providing a 0.15-m footprint. The waveforms incident on the live and the dead tree were carefully selected and extracted from each swath to enable the precise LAI_e estimation of the live tree and CHP generation of the dead tree.

For four of the swaths (24, 76, 82, and 86), the trees were located at the swath's edge, at large incidence angles (18°–24°) (see Fig. 2). For the remaining two swaths (29 and 41), the trees were situated at the center and therefore sampled nearly at nadir. Swaths 24, 29, 82, and 86 were flown due northwest. The trees in swaths 24 and 86 were situated on the SW edge of that swath, causing the south of the trees to be obscured and not sampled well. In swath 29, the trees were in the center of the swath, whereas in swath 82, the trees were on the NE edge of the swath, causing the north side of the tree to be obscured. Swath 41 was flown from south to north with the trees at the center of the swath. The flight line of swath 76 was from northwest to southeast with the trees on the southern edge of the swath, again causing the south of the trees to be undersampled. Therefore, what the LiDAR captured in swaths 24, 76, and 86 was quite different to the capture of swath 82. The remaining two swaths, acquired at nearly nadir, provided the most even description of tree structure.

III. Methods

A. Convergent Photographs

The preprocessing of convergent photographs was undertaken using the commercial software PhotoModeler (Eos Systems Inc.). Calibration of the camera was performed using 12 photographs of the calibration grid taken prior to fieldwork and processed according to the PhotoModeler instructions [13]. The overall root mean square error (RMSE) of the camera calibration was 0.33 pixels, and the camera focal length of 35.29 mm was obtained.

With the calibration parameters known, homologous points were referenced in convergent photographs, allowing the position and orientation of each photograph to be determined (calculation of the camera position by resection). The scale and orientation of the model was set using the GPS measurement of four fence posts located nearby and visible in the images. This was then verified by checking the length of a 1-m ruler placed on site during the field visit. The length of the ruler was found to be accurate to within 1 cm. The final PhotoModeler

photo-orientation project of the forest scene was solving well with the overall RMSE of 0.40 pixels (i.e., for photographs taken 18 m away from the target, this equates to approximately 2 mm).

Using the orientated photographs, the structure of both trees was reconstructed by measuring corresponding tree points. Reconstruction was relatively easy in the case of the dead tree. However, due to obstruction by the foliage, the reconstruction of the structure of the live *Callitris glaucophylla* tree was much more difficult. Fig. 1 shows the result of this reconstruction. Since the dead tree had its structure represented better than the live tree, the histogram of its points was used for the validation of LiDAR CHP.

It needs to be mentioned that the presented method of tree structure reconstruction has its drawbacks. The main problem was the wind causing the trees to move and therefore shifting them between photographs. A way to solve this problem would be to use synchronized cameras and, possibly, to capture the photographs as stereo pairs. Furthermore, the measurement of homologous points was limited due to difficulty in identifying the same parts of the tree from different angles of convergent photographs. The point distribution was also dependent on the degree of occlusions and was subject to the operator's choice of homologous points (random, rather than in an irregular grid as in the case of LiDAR).

B. Hemispherical Photography

Hemispherical photographs (also called fish-eye photographs) were processed to obtain an estimate of $\mathrm{LAI_e}$ of the live tree using HemiView software with the "single tree" option. Field-measured tree height and crown radius estimated based on the PhotoModeler model were used as input values. A half ellipse was chosen as the best tree shape approximation. Due to some obstructions present in the photographs, the original images were masked out to hide everything that did not represent the crown of the tree and to match the selected LiDAR data as closely as possible. Only the part of the photograph tangent to the crown was taken into account. The $\mathrm{LAI_e}$ estimates for each of the four photographs were averaged to produce the final fish-eye lens $\mathrm{LAI_e}$ value of the live tree.

C. LiDAR Data

All LiDAR swaths were processed to detect peaks in waveforms and optimized with a trust-region-reflective algorithm using the custom decomposition procedure described in [14]. For each data set, a digital terrain model (DTM) was produced from single returns classified as ground and was used together with the original waveform amplitude train, and it optimized parameters of peaks in the CHP methodology [7], [11]. The LiDAR $\mathrm{LAI_e}$ of the live tree was derived from raw waveform (as a step in CHP) and from discrete points extracted from the waveform. All $\mathrm{LAI_e}$ retrievals were then compared to the estimates from the fish-eye photography. The calculations of $\mathrm{LAI_e}$ and CHP were performed separately for each of the six swaths as well as for the combined data set of the six swaths. The CHP of the dead tree was validated against the PhotoModeler tree profile using binwise ordinary least square regression (15-cm height bins). Since the profiles represent the relative distribution of vegetation, the RMSE was normalized by the maximum bin value in the PhotoModeler profile to provide normalized $\mathrm{RMSE_{norm}}$.

1) Raw-Waveform LAI and CHP: The purpose of the CHP methodology was to represent the distribution of foliage more accurately than raw waveform, by scaling up return energy with increasing range to account for the fact that less energy is incident for the later returns. The CHP procedure is performed in five stages: waveform alignment, returned energy profile, canopy closure profile, cumulative leaf (plant) area index profile, and CHP. The details of this methodology adapted to the small-footprint airborne scanner can be found in [11].

The CHP procedure was applied twice with different reflectance ratio values producing two estimates of $\mathrm{LAI_e}$ from raw waveform and two CHPs. Since the ground is approximately twice as reflective as vegetation at the laser wavelength (1550 nm), an arbitrary ratio of 0.5 was used initially (WF1). The soil in the study area is a mixture of sand, silt, and clay. Taking a mean reflectance of those three soils (according to Bowker *et al.* [15]) at a LiDAR wavelength of 1550 nm and estimating the typical reflectance of vegetation, the ratio between vegetation and the ground is around 0.4. The computation of the Gillenbah forest study-area-adjusted reflectance ratio was performed based on the procedure proposed in [16] and proved consistent with what could be predicted for the soil in the study area. The ratio of 0.42 was therefore used in the second method (WF2).

2) Discrete Point LAI_e: The point clouds resulting from the custom decomposition, after DTM subtraction, were used to provide a discrete point $\mathrm{LAI_e}$ derived from the gap probability. Two gap probability (P) ratios were tested: 1) single ground returns (< 0.5 m) over total number of waveforms incident on the tree (PT1) and 2) all ground returns (< 0.5 m) over total number of points extracted from waveforms (PT2). The $\mathrm{LAI_e}$ was then calculated as the negative natural logarithm of this probability according to [5]

$$\mathrm{LAI_e} = -\ln(P). \tag{1}$$

IV. Results and Discussion

A. LAI_e

The fish-eye $\mathrm{LAI_e}$ of the live *Callitris glaucophylla* tree obtained as a mean value of four photographs yielded 1.87 with a standard deviation of 0.18 and a standard error of the mean of 0.09 (see Table I). This $\mathrm{LAI_e}$ estimate was compared to the LiDAR-derived estimates using raw waveform (WF) and discrete point (PT) methods (see Table I). The LiDAR estimates were obtained in two ways: 1) as a mean value of six swaths processed separately to obtain $\mathrm{LAI_e}$ and 2) by combining the swaths prior to the computation of $\mathrm{LAI_e}$. When the $\mathrm{LAI_e}$ was computed as the mean of six swaths, PT1 and WF1 performed best, providing estimates very close to that of the fish-eye photograph (within -1.8%). For combined swaths, the best results were obtained by point method PT1 (-1.3%)

TABLE I
COMPARISON OF LiDAR AND FISH-EYE LAI_e

	FEYE	WF1	WF2	PT1	PT2
MEAN	1.87	1.83 (-1.8%)	1.98 (+6.1%)	1.83 (-1.6%)	1.99 (+6.9%)
ST.DEV	0.18	0.22	0.23	0.34	0.15
SEM	0.09	0.09	0.09	0.14	0.06
COMBINED	1.87	1.76 (-5.4%)	1.92 (+2.9%)	1.84 (-1.3%)	1.99 (+6.8%)

FEYE- fish-eye method; WF1 - waveform method with reflectance ratio of 0.5; WF2 - waveform method with reflectance ratio of 0.42. PT1 - point method with single ground returns. PT2 - point method with all ground returns. MEAN – mean value of six swaths or four fish-eye photographs; ST DEV – standard deviation; SEM – standard error of the mean.

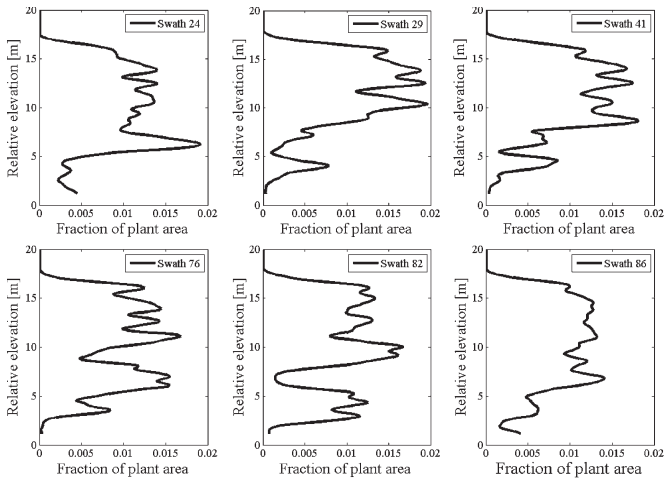

Fig. 3. CHP of the live *Callitris glaucophylla* for six swaths.

followed by waveform method WF2 with a 0.42 reflectance ratio (+2.9%). Despite having results that matched the closest those of the fish-eye photograph, PT1 had the highest standard deviation of all methods. WF1 and PT1 underestimated whereas WF2 and PT2 overestimated the fish-eye LAI_e. However, the magnitude of over- and underestimation in this study is very low ($\pm$7%) and within the standard deviations calculated from six swaths. Nevertheless, in general, all methods performed very well, providing mean LAI_e values within $\pm$7% of the fish-eye estimate.

In the case of such small data sets, the precise estimation of LAI_e is strongly dependent on the selection of the waveforms/points incident on the tree, limiting the area of interest to crown extents. Due to the logarithmic transformation applied to compensate for the effect of occlusion, the LAI_e does not scale linearly. Thus, selecting the area larger than the tree crown will lead to the underestimation of the tree LAI_e.

B. CHP

The CHP from the live tree for each swath is presented in Fig. 3. The plots from swaths 29 and 41 are the most similar to each other as they were both captured almost at nadir angle. Swaths 24, 76, and 86, since they were scanned from a similar

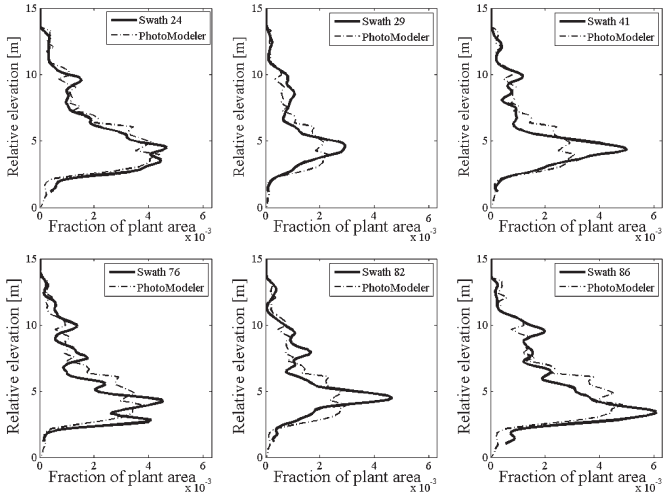

Fig. 4. Normalized CHP of the dead *Callitris glaucophylla* tree for six swaths with PhotoModeler profile overlaid.

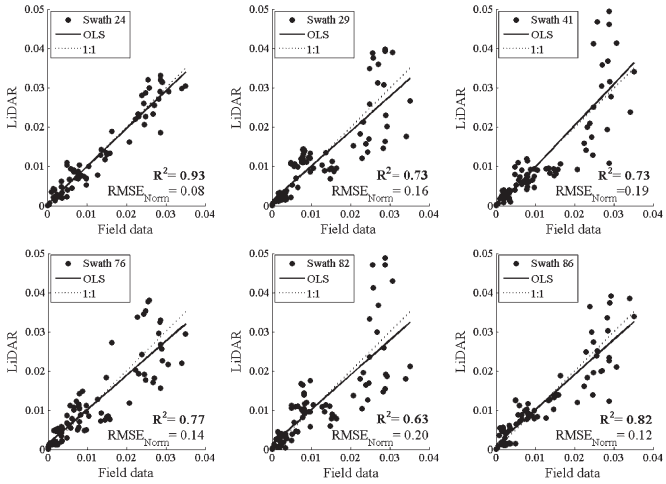

Fig. 5. Dead tree binwise CHP regression against PhotoModeler profile for six swaths.

direction, seemed to have picked up a feature (branch) on the north side of the tree between 6 and 8 m AGL. This branch was completely missed by swaths 29, 41, and 82. Conversely, swath 82 recorded vegetation between 2 and 6 m above the ground, on the south side of the tree, which was completely missed by swath 24 and only partially captured in swaths 29, 41, 76, and 86. All these differences prove that the angle of incidence has an important influence on what LiDAR "can see," when analyzing very small data sets or discontinuous canopies.

Since the validation of the tree structure of the live tree was not possible due to limitations of the photoreconstruction, the CHP is validated against the dead tree PhotoModeler profile. The comparison was performed for each swath (see Fig. 4) and for the combined profile [Fig. 6 (left)]. Since two reflectance ratios showed very similar results with marginal improvement for the ratio of 0.42, only results of this method are provided. To compare the CHP and PhotoModeler profiles, binwise ordinary least square regression was carried out (Fig. 5).

The LiDAR CHP closely follows the profile of PhotoModeler, particularly in the case of swath 24, for which the correlation reaches an excellent maximum R^2 of 0.93 and the lowest

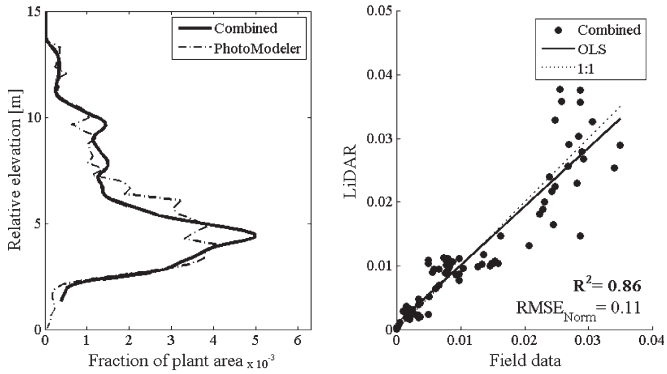

Fig. 6. (Left) Dead tree combined-swath CHP and (right) its binwise regression against the PhotoModeler.

normalized $\mathrm{RMSE}_{\mathrm{norm}}$ of 8%. Swath 86 provided the second best result with a R^2 of 0.82 and a $\mathrm{RMSE}_{\mathrm{norm}}$ of 12%. In the case of swath 76, the shape of the profile is also preserved, but with some bias causing the R^2 to drop to 0.77 and a higher $\mathrm{RMSE}_{\mathrm{norm}}$ of 14%. Nevertheless, the two swaths that captured the north of the tree provided the highest correlation with the PhotoModeler profile. For the remaining swaths, LiDAR seems to have picked up more returns around 5 m AGL, causing the overestimation of the PhotoModeler profile. For the swaths acquired nearly at nadir (29 and 41), the correlation was the same, yielding a R^2 of 0.73. Swath 82, the only one which had the north of the tree obscured, provided the lowest (R^2 of 0.63) but still significant correlation with the PhotoModeler profile. Finally, for the six combined swaths, the correlation yielded an excellent R^2 of 0.86 with a $\mathrm{RMSE}_{\mathrm{norm}}$ of 11% (see Fig. 6). Additionally, all regression lines were very close to the $1:1$ line.

The dead tree is not symmetrical, and most of its branches are on its north side, whereas the southeast side of the tree is branchless. This explains why the correlation of swaths depicting the north side of the tree in detail gave the highest correlation and why swath 82 yielded the lowest correlation. The two swaths acquired at nadir should provide the most objective profile of the tree and, theoretically, better correlation than the swaths 24 and 76. This is where the accuracy of the PhotoModeler profile comes into the picture. The lower parts of the tree, where a lot of twigs were present, were difficult to identify in Photomodeler. Therefore, some might have been missed, causing underestimation of the ground-truth profile around 5 m AGL.

V. Conclusion

This letter has presented a study of the CHP methodology applied at a single-tree level to derive $\mathrm{LAI_e}$ and the vertical tree profile. The methodology proved successful in deriving the $\mathrm{LAI_e}$ of a single *Callitris glaucophylla* tree, providing very close results to those of hemispherical photography ($\pm 7\%$) as well as to discrete point methods of estimation of this parameter. The comparison of the LiDAR vertical tree profile (CHP) to the PhotoModeler-generated "field" profile also showed very high correlation between the data (R^2 of 0.86 for combined swaths), giving some confidence in the suitability of the approach. Using a site-specific vegetation-ground reflectance ratio as opposed to 0.5 for the laser wavelength of 1550 nm in CHP generation provided marginal improvement in the correlation between the profiles.

The methodology was applied to six different swaths of data, acquired at different angles, and to the combined data of all six swaths. This showed some differences in the estimation of the vegetation profile depending on the scanning angle and reiterated its importance. Further work should therefore focus on investigation of the influence of the scanning angle on larger scale retrievals. The validation of the CHP methodology for $\mathrm{LAI_e}$ and vegetation profile estimation of other tree species should also be considered.

References

[1] B. Koetz, F. Morsdorf, G. Sun, K. J. Ranson, K. Itten, and B. Allgöwer, "Inversion of a LiDAR waveform model for forest biophysical parameter estimation," *IEEE Geosci. Remote Sens. Lett.*, vol. 3, no. 1, pp. 49–53, Jan. 2006.

[2] I. Jonckheere, S. Fleck, K. Nackaerts, B. Muys, P. Coppin, M. Weiss, and F. Baret, "Review of methods for in situ leaf area index determination: Part I. Theories, sensors and hemispherical photography," *Agric. Forest Meteorol.*, vol. 121, no. 1/2, pp. 19–35, Jan. 2004.

[3] P. E. Levy and P. G. Jarvis, "Direct and indirect measurements of LAI in millet and fallow vegetation in HAPEX-Sahel," *Agric. Forest Meteorol.*, vol. 97, no. 3, pp. 199–212, Nov. 1999.

[4] A. R. G. Lang, R. E. McMurtrie, and M. L. Benson, "Validity of surface area indices of Pinus radiata estimated from transmittance of the sun's beam," *Agric. Forest Meteorol.*, vol. 57, no. 1–3, pp. 157–170, Dec. 1991.

[5] J. D. Aber, "Method for estimating foliage-height profiles in broad-leaved forests," *J. Ecol.*, vol. 67, no. 1, pp. 35–40, Mar. 1979.

[6] R. H. MacArthur and H. S. Horn, "Foliage profile by vertical measurements," *Ecology*, vol. 50, no. 5, pp. 802–804, Sep. 1969.

[7] D. J. Harding, M. A. Lefsky, G. G. Parker, and J. B. Blair, "Laser altimeter canopy height profiles: Methods and validation for closed-canopy, broadleaf forests," *Remote Sens. Environ.*, vol. 76, no. 3, pp. 283–297, 2001.

[8] M. A. Lefsky, W. B. Cohen, S. A. Acker, G. G. Parker, T. A. Spies, and D. Harding, "Lidar remote sensing of the canopy structure and biophysical properties of Douglas-fir western hemlock forests," *Remote Sens. Environ.*, vol. 70, no. 3, pp. 339–361, Dec. 1999.

[9] J. B. Blair and M. A. Hofton, "Modeling laser altimeter return waveforms over complex vegetation using high-resolution elevation data," *Geophys. Res. Lett.*, vol. 26, no. 16, pp. 2509–2512, Aug. 1999.

[10] T. A. Black, J.-M. Chen, X. Lee, and R. M. Sagar, "Characteristics of shortwave and longwave irradiances under a Douglas-fir forest stand," *Can. J. Forest Res.*, vol. 21, no. 7, pp. 1020–1028, Jul. 1991.

[11] K. D. Fieber, I. J. Davenport, M. A. Tanase, J. M. Ferryman, R. J. Gurney, J. P. Walker, and J. M. Hacker, "Preliminary leaf area index estimates from airborne small-footprint full-waveform lidar data," in *Proc. IEEE IGARSS*, Melbourne, VIC, Australia, 2013, pp. 3379–3382.

[12] R. Panciera, J. P. Walker, T. J. Jackson, D. A. Gray, M. A. Tanase, D. Ryu, A. Monerris, H. Yardley, C. Rudiger, X. Wu, Y. Gao, and J. M. Hacker, "The soil moisture active passive experiments (SMAPEx): Toward soil moisture retrieval from the SMAP mission," *IEEE Trans. Geosci. Remote Sens.*, vol. 52, no. 1, pp. 490–507, Jan. 2014.

[13] PhotoModeler Software Website 2013. [Online]. Available: http://www.photomodeler.com

[14] K. D. Fieber, I. J. Davenport, J. M. Ferryman, R. J. Gurney, J. P. Walker, and J. M. Hacker, "Analysis of full-waveform LiDAR data for classification of an orange orchard scene," *ISPRS J. Photogramm.*, vol. 82, pp. 63–82, Aug. 2013.

[15] D. Bowker, R. Davis, D. Myrick, K. Stacy, and W. Jones, "Spectral reflectances of natural targets for use in remote sensing studies," NASA, Washington, DC, USA, Rep. RP-11391985, Jun. 1985.

[16] J. Armston, M. Disney, P. Lewis, P. Scarth, S. Phinn, R. Lucas, P. Bunting, and N. Goodwin, "Direct retrieval of canopy gap probability using airborne waveform lidar," *Remote Sens. Environ.*, vol. 134, pp. 24–38, Jul. 2013.